

ORNL
MASTER COPY

11
DATE ISSUED OCT 17 1980

OAK RIDGE NATIONAL LABORATORY

OPERATED BY
UNION CARBIDE CORPORATION
NUCLEAR DIVISION



POST OFFICE BOX X
OAK RIDGE, TENNESSEE 37830

SPECIAL DISTRIBUTION

ORNL
CENTRAL FILES NUMBER

ORNL/CF-80/304

801010

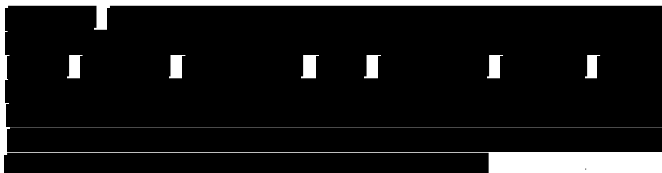
DATE: October 7, 1980

SUBJECT: Technical Highlights of Space and Terrestrial Systems Programs
at Oak Ridge National Laboratory for June 1980

TO: Distribution

FROM: R. H. Cooper

This monthly report is intended to inform the Space and Terrestrial Systems Division, DOE, and their contractors of significant technical highlights of technology and systems support programs in progress at Oak Ridge National Laboratory. A detailed technical presentation of information will be published in topical reports and open literature publications.



CONTENTS

INTERNATIONAL SOLAR-POLAR MISSION MATERIALS SUPPORT.....	1
CBCF-3 Fabrication	1
CBCF-3 Characterization	3
Creep Properties of 2219 Aluminum Housing Materials	11
Important Meetings	18
FLIGHT SYSTEMS HARDWARE	19
Iridium Forming Blank Fabrication	19
Meetings	20
MATERIALS TECHNOLOGY SUPPORT	21
Effect of Oxidizing Environment on GPHS Impact Temperature Margin	21
Effect of Test Temperature on Tensile Properties of As-Rolled DOP-26 Production material	25
Effect of Stress-Relief Temperature on Room-Temperature Tensile Properties of DOP-26 Production Material	25
Slow Strain Rate Tensile Properties of Pt-30 Rh Alloy	29
Bonding of (Cu,Ag) ₂ Se to W-25% Re	30
ISOTOPE FUEL DEVELOPMENT	33
⁹⁰ SrF ₂ Compatibility	33
TERRESTRIAL RADIOISOTOPE APPLICATION DEVELOPMENT	34
Cesium-137 Low Solubility Compounds	34
Krypton-85 Light Source Development	35
BENEFICIAL APPLICATIONS OF RADIATION TECHNOLOGY	36

INTERNATIONAL SOLAR-POLAR MISSION MATERIALS SUPPORT

(Activity AE 15 15 20 0, WPAS 02313)

R. L. Heestand

The purpose of this task is to provide direct materials support on work specific to the General Purpose Heat Source (GPHS) design. The scope of this work includes (1) determining the impact properties and optimum weld parameters for the DOP-26 iridium alloy fuel cladding material, (2) thermal conductivity and emissivity data on cladding and thermal insulation materials, (3) fabrication and characterization of carbon-bonded carbon-fiber (CBCF) insulation developed by ORNL and Y-12 for GPHS, and (4) determination of creep properties of the 2219 aluminum alloy housing. Data on the impact properties and welding of iridium are integrated with complementary work reported in the Materials Technology section of this report.

CBCF-3 Fabrication (G. W. Brassell,* R. L. Heestand, C. Hamby, G. C. Wei, and R. L. Beatty)

To date, a total of 16 multiple-mandrel runs have been completed at the ORNL CBCF-3 fabrication facility. Table 1 summarizes the results of these runs. Several types of defects including cracks, large pores, and high-density inclusions in the carbonized billets were observed. The cracking problem probably is related to the residual water content in the mold and the drying and curing process. This problem has been approached by better control of the dewatering process. The numerous large pores observed in nearly all the molds except billets C-6's were eliminated by (1) increasing the water level in the molding tank to reduce the amount of air trapped in the water due to the transferring of the fiber-resin-water slurry from the slurry tank to the molding tank, and (2) stopping the agitation in the slurry tank for two minutes before the molding to let gas bubbles escape while maintaining a reasonably homogeneous slurry. The high-density inclusions observed in all the billets were minimized to only a few inclusions per billet by thoroughly rinsing of the slurry and molding tanks before slurry preparation and molding.

It should be noted that the carbonization of billets C-8's and thereafter was at 1600°C for 3 h in flowing argon. This carbonization process is selected instead of the conventional (1350°C for 3 h) carbonization process because the billets are dimensionally stable during the 1500°C/36 h/5.0E-5 torr outgassing. The effect of increasing the carbonization temperature from 1350°C to 1600°C on the thermal conductivity of the carbonized parts is expected to be minor because Taylor's flash

*Now with Rocky Flat Weapons Plant, Golden, Colorado.

Table 1. Results of CBCF-3 Fabrication at ORNL

Run	Carbonization		Results
	Temperature (°C)	Time (h)	
C-1	1500	1	large pores and high-density inclusions in 9 billets
C-2	1500	1	large pores and high-density inclusions in 9 billets
C-3	1500	1	cracks, large pores, and high-density inclusions in 9 billets
C-4	1500	1	cracks in 4 billets, large pores and high-density inclusions in 9 billets
C-5	1500	1	cracks in 3 billets, large pores and high-density inclusions in 9 billets
C-6	1550	3	a few high-density inclusions in 9 billets, no pores or cracks
C-7	1550	3	large pores and a few high-density inclusions in 9 billets
C-8	1600	3	large pores and a few high-density inclusions in 9 billets
C-9	1600	3	large pores and a few high-density inclusions in 9 billets
C-10	1600	3	large pores and a few high-density inclusions in 9 billets
C-11	1600	3	large pores and a few high-density inclusions in 9 billets
C-12	1600	3	large pores and a few high-density inclusions in 9 billets
C-13	1600	3	large pores and a few high-density inclusions in 9 billets
C-14	1600	3	large pores and a few high-density inclusions in 9 billets
C-15	1600	3	no pores, a few high-density inclusions in 9 billets, cracks in 6 billets
C-16	1600	3	(in inspection)
P-1	1500	1	some high-density inclusions but no pores or cracks.

diffusivity measurements of outgassed CBCF-3 cups ($0.20E3 \text{ kg/m}^3$ and carbonized at 1350°C for 3 h) showed less than a 5% increase in the thermal conductivity at 1600°C in vacuum after heating the specimen from 1600°C to 2000°C and cooling to 1600°C for a total time of 1 h.

Machining of CBCF-3 billets including tubes C-6-2, -4, -5, -6; C-8-2, -3, -4, -5, -7, -8, -9; C-15-2, -4, -7; and plates P-C-2, P-C-3 at an outside firm is in process. The machined parts will be used in GE's vibration tests and LASL's design verification tests and the test samples will be used in the thermal conductivity measurements. Tubes C-6-7, -8, -9 were delivered to LASL for their demonstration of machining of this material. Tubes C-10-1 to 7, and C-9-1 to 7 were sent to TECO for machining of parts and test samples.

Machined parts and unmachined billets fabricated at Y-12 were reviewed. Table 2 lists these materials. Some of these materials including six machined sleeves, 19 unmachined cups, one unmachined plate, 32 machined disks are being reworked for possible use in the GPHS program.

A purchase order of the chopping of 550 kg of rayon filaments (made by Beaunit Rayon Co., Elizabethton, TN) to specified lengths was placed at Microfiber Co., Pawtucket, RI. This batch of chopped rayon fibers will be used as a back-up batch for the AEPC-2 batch of carbon fiber for the GPHS program.

CBCF-3 Characterization (G. C. Wei)

Dimensional stability of CBCF-3 tubes during the $1500^\circ\text{C}/36 \text{ h}/5.0E-5$ torr outgassing was studied. No measurable changes in dimensions were observed during the outgassing of the CBCF-3 tubes carbonized at 1550°C or 1600°C for 3 h. Additional four CBCF-3 tubes carbonized at 1600°C for 3 h will be outgassed to fully establish the dimensional stability of CBCF-3 parts.

Thermal conductivity specimens from six CBCF-3 cups (with two each from three multi-mandrel runs) and two CBCF-3 plates fabricated at Y-12 and carbonized at 1350°C for 3 h and outgassed ($1500^\circ\text{C}/36 \text{ h}/5.0E-5$ torr) were sent to TPRL of Purdue University for thermal conductivity determinations. These specimens have densities ranging from 0.18 to $0.22E3 \text{ kg/m}^3$. Preliminary results of the thermal conductivity measurements indicate a $\pm 45\%$ variation in the room-temperature thermal conductivity in vacuum. High-temperature thermal conductivity measurements of these samples are in process. Additional thermal conductivity specimens from CBCF-3 billets fabricated at ORNL and carbonized at 1600°C for 3 h are being prepared.

Chemical analyses including ash analysis and spark source mass spectroscopic analysis of outgassed CBCF-3 materials fabricated at ORNL and Y-12 were performed. The results of ash analyses of outgassed samples from CBCF-3 cups 77, 78, 79, 82, 84, 92, 94, 98, 100, 104, 105, 119, and plates 1, 4 (fabricated at Y-12) and CBCF-3 tubes C-1-1, C-6-1, C-7-1, and

Table 2. CBCF-3 Materials (Y-12 Fabricated) on Hand

Type	Part No. ^a	Critical Dimensional Nonconformance ^b	Radiography Results
Machined Sleeves	7885-50-1670	None	cracks, high-density inclusions
	(*)7885-50-1681	ID,+0.010	high-density inclusions
	(*)7885-50-1686	ID,+0.004	high-density inclusions
	(*)7885-50-1687	ID,+0.004	high-density inclusions
	7885-50-1685/7893-14-9665	OD, -0.004; O, 0.004; L, -0.007	cracks, high-density inclusions
	(*)7885-50-1764/7893-14-9666	O, 0.005; L, -0.009	high-density inclusions
	(*)7886-36-2184/7893-14-9667	OD,+0.009	high-density inclusions
	7886-36-2185/7893-14-9668	OD, -0.004	cracks, high-density inclusions
	(*)7886-36-2187/7893-14-9669	L, -0.012	high-density inclusions
	7886-36-2188/7893-14-9670	OD,+0.009; L, -0.005	cracks, high-density inclusions
	7886-36-2189/7893-14-9671	O, 0.005	cracks, high-density inclusions
	7886-36-2190/7893-14-9672	L, -0.004	cracks, high-density inclusions
	(*)7886-36-2191/7893-14-9673	L, -0.0014	high-density inclusions

Table 2. (continued)

Type	Part No. ^a	Critical Dimensional Nonconformance ^b	Radiography Results
	7893-16-6551	0, 0.004	pores and high-density inclusions
	7893-16-6552	0, 0.004; L, -0.005	pores and high-density inclusions
	7893-16-6553	L, -0.009	pores and high-density inclusions
	7893-16-6554	L, -0.010	pores and high-density inclusions
	7893-16-6555	0, 0.003	pores and high-density inclusions
	7893-16-6556	L, -0.009	pores and high-density inclusions
	7893-16-6557	L, -0.010	cracks, pores, and high-density inclusions
	7893-16-6558	L, -0.012	pores and high-density inclusions
		<u>Density^c</u>	
Machined Disks	(*)7787-29-5819	—	high-density particles and areas
	(*)7787-29-5848	—	high-density particles and areas
	(*)7893-27-6563	0.245	in inspection
	(*)7893-27-6564	0.248	in inspection
	(*)7893-27-6565	0.232	in inspection
	(*)7893-27-6566	0.235	in inspection

Table 2. (continued)

Type	Part No. ^a	Critical Dimensional Nonconformance ^b	Radiography Results
		<u>Density</u>	
	(*)7893-27-6567	0.238	in inspection
	(*)7893-27-6568	0.222	in inspection
	(*)7893-27-6569	0.228	in inspection
	(*)7893-27-6570	0.253	in inspection
	(*)7893-27-6571	0.250	in inspection
	(*)7893-27-6572	0.251	in inspection
	(*)7893-27-6573	0.223	in inspection
	(*)7893-27-6574	0.259	in inspection
	(*)7885-52-1688	0.23	high-density particles and areas
	(*)7885-52-1689	0.22	high-density particles and areas
	(*)7885-52-1690	0.23	high-density particles and areas
	(*)7885-52-1691	0.23	high-density particles and areas
	(*)7885-52-1692	0.22	high-density particles and areas
	(*)7885-52-1693	0.22	high-density particles and areas
	(*)7885-52-1717	0.247	high-density particles and areas

Table 2. (continued)

Type	Part No. ^a	Critical Dimensional Nonconformance ^b	Radiography Results
		<u>Density</u>	
	(*)7885-52-1718	0.252	high-density particles and areas
	(*)7885-52-1719	0.246	high-density particles and areas
	(*)7885-52-1720	0.245	high-density particles and areas
	(*)7885-52-1721	0.249	high-density particles and areas
	(*)7885-52-1723	0.238	high-density particles and areas
	(*)7885-52-1724	0.239	high-density particles
	(*)7885-52-1725	0.250	high-density particles
	(*)7885-52-1727	0.245	high-density particles and areas
	(*)7885-52-1728	0.228	high-density particles and areas
	(*)7885-52-1729	0.245	high-density particles and areas
	(*)7885-52-1737	0.261	high-density particles and areas
		<u>Carbonization</u>	
Unmachined Cups	120	1500°C/3 h	pores and high-density particles
	121	1500°C/3 h	pores and high-density particles

Table 2. (continued)

Type	Part No. ^a	Critical Dimensional Nonconformance ^b	Radiography Results
		<u>Carbonization</u>	
	122	1500°C/3 h	cracks, pores, and high-density particles
	123	1500°C/3 h	cracks, pores, and high-density particles
	124	1500°C/3 h	pores and high-density particles
(*)	125	1500°C/3 h	high-density particles
	126	1500°C/3 h	cracks, pores, and high-density
(*)	127	1500°C/3 h	high-density particles
	128	1500°C/3 h	pores and high-density particles
(*)	130	1500°C/3 h	high-density particles
(*)	131	1500°C/3 h	high-density particles
(*)	132	1500°C/3 h	high-density particles
(*)	133	1500°C/3 h	high-density particles
(*)	134	1500°C/3 h	high-density particles
(*)	135	1500°C/3 h	high-density particles
(*)	136	1500°C/3 h	high-density particles
(*)	137	1500°C/3 h	high-density particles
	78	1350°C/3 h	cracks, pores, and high-density particles

Table 2. (continued)

Type	Part No. ^a	Critical Dimensional Nonconformance ^b	Radiography Results
		<u>Carbonization</u>	
	(*) 89	1350°C/3 h	high-density particles
	(*) 94	1350°C/3 h	high-density particles
	(*) 100	1350°C/3 h	high-density particles
	(*) 101	1350°C/3 h	high-density particles
	(*) 106	1350°C/3 h	high-density particles
	(*) 107	1350°C/3 h	high-density particles
	(*) 108	1350°C/3 h	high-density particles
	109	1350°C/3 h	pores and high-density particles
	(*) 110	1350°C/3 h	high-density particles
	(*) 119	1350°C/3 h	high-density particles
Unmachined Plates	5	1500°C/3 h	cracks and high-density particles
	6	1500°C/3 h	high-density particles

^aParts marked "(*)" are being heat-treated at 1600°C for 3 h.

^bDimensions of the sleeve were specified as OD, 1.715 ± 0.002 ; ID, 1.555 ± 0.002 ; O, 0.002 ; L, 3.000 ± 0.002 , where O means concentricity, L means length, and dimensions are in inches.

^cDensities of most machined disks were out of specification probably because of excessive binders.

C-8-7 (fabricated at ORNL) indicated the ash contents all less than 0.3% as specified in Mound Facility's CBCF-3 specification. Spark source mass spectroscopic analyses of trace impurities in outgassed samples from Y-12 CBCF-3 materials (cup 78, 82, 85, 86, 87, 94, 98, 100, 101, and plate 1, 4) showed the following impurities higher than the specified limits, Ti, Ca, S, Si, and B. However, the spark source chemical analyses of outgassed CBCF-3 samples (fabricated at ORNL) from billets C-1-1 and C-6-1 showed only Ti and S were above the specification limit. All other elements were within the specification limit. The source of Ti and S in the ORNL-fabricated parts may be related to the graphite components in the carbonization furnace. A high-temperature bake-out of the furnace may eliminate the Ti and S contamination.

The bulk density of the CBCF-3 tubes and plates fabricated at ORNL is in the range of 0.19 to 0.22E3 kg/m³. Therefore, the density of the ORNL-fabricated billets meets the specification. Sleeves machined from CBCF-3 cups 111 to 118 (fabricated at Y-12) have densities from 0.19 to 0.22E3 kg/m³ but the associated test samples showed densities of 0.22 to 0.24E3 kg/m³ and compressive strengths of 0.66 MPa (96 psi) to 0.793 MPa (115 psi). The densities of these test samples are higher than the specification limit probably due to improper machining procedures used in the machining of these test samples. The outside firm who is currently involved in the machining of test samples and sleeves from CBCF-3 tubes has been informed with proper machining procedures and sleeves and test samples of correct densities are anticipated.

In this period, considerable amount of time was spent on identification of the causes of defects including large pores and high-density inclusions in the ORNL-fabricated tubes. Radiography was used extensively in the examinations of these defects. Numerous pores up to 2 mm in diameter were observed in carbonized parts. Radiographic examination of as-cured parts indicated numerous pores especially in the top portion of the as-cured parts. Therefore, the presence of large pores was not related to carbonization, but due to molding and/or slurry preparation. The molding and slurry preparation process was then critically reviewed. Review of process records of the CBCF-3 cups (made at Y-12) of which some had large pores but some not and the CBCF-3 tubes (fabricated at ORNL) which had large pores in all except billets C-6's did not reveal any clues as to critical parameters controlling the generation of the large pores. Large agglomerates of resin particles were thought to be one possible source of the large pores but they were ruled out after parts which were made using sieved resin particles still showed the presence of large pores. The fact that most of the pores were located in the top portion of the tubes suggests that increasing the water level in the molding tank may be helpful in eliminating the pores. Exceedingly long dewatering time up to 15 minutes or more due to the reuse of filter cloth and the limited vacuum capacity because of the small size of the holding tank was thought to be possible factors contributing to the presence of large pores. However, after using new filter cloth, improving the vacuum capacity of the molding system, the dewatering times was reduced to less than a minute but the pores were still observed in the parts.

Creep Properties of 2219 Aluminum Housing Materials (J. P. Hammond)

The purpose of this task is to develop creep design curves on the 2219-T6 aluminum forging and to aid GE, Valley Forge, in the design of the shell component of the RTG generator. The essential requirement of the shell will be to firmly retain the RTG generator under elastic stress during ground tests and storage in air (condition II), and subsequent flight in vacuum (condition I).

Test specimens were provided from the end cropping of the 2219-T6 forging from which the shell will be fabricated and General Electric, Valley Forge, communicated an agreed-on creep test matrix, given in Table 3. General Electric is conducting tensile and metallographic tests to characterize the forging and provide tensile data. The creep test matrix calls for two proof tests to evaluate the magnitude of creep strain under the worst stress-temperature situations envisioned for the shell during the 10,000 h (518°F) flight in space (Test I, Table 3) and the combined ground test (518°F) and 10,000 h storage at 350°F (Test II), respectively. It is understood that the total creep strain from tests I and II combined should not exceed 0.4%. Further, to evaluate any safety margin provided by limitations on stress, design curves establishing the stress-time relationships for 0.2% and 0.1% creep at 500 and 350°F were to be determined.

The results of the creep tests conducted to date are given in Table 4. Total creep strain (ϵ_p) for the time in test (t) are given along with the constant rate of secondary creep ($\dot{\epsilon}_m$). The latter is only given where it appeared that the steady state may have been attained. Even so, the $\dot{\epsilon}_m$ values must be taken as tentative (usually biased to high values) in view of the short durations of test.

The computer readout creep curves for proof tests I and II are shown in Figs. 1 and 2, respectively. Indications of the stages of creep response are marked on the graphs along with the computations of $\dot{\epsilon}_m$. Proof test I, which is a 10,000 h exposure at 518°F under 5 ksi stress (space flight) shows a primary stage of creep from A to B and seemingly secondary creep from B to C, for which the constant rate of creep is $6.6 \times 10^{-7}/h$. The total creep strain through the present 955 h of testing is 0.116%. However, 9045 h remain to complete the test and computation shows that the specimen will ultimately strain to 0.713% if the present value for $\dot{\epsilon}_m$ is maintained. Disregarding the primary stage of creep, an $\dot{\epsilon}_m$ value of $2.0 \times 10^{-7}/h$ would be required to limit total strain to 0.2% during the 10,000 h period.

Proof test II, which consists of 600 h pretest age at 518°F under 3.5 ksi stress followed by 10,000 h storage at 350°F (on ground), has presently logged 1504 h and has crept a total of 0.108% (Table 4). The region A-B in Fig. 2 represents the creep response during on ground aging, B-C shows the strain sustained from taking the test from the aging to the storage condition, and C-D-E gives the creep response during the first 900 h of the storage period. It would appear that the strain from A to D in Fig. 2 is essentially primary creep and D-E is

Table 3. Al 2219-T6 Alloy Creep Test Matrix

Test	Pretest Age	Test Temp (°F)	Stress (psi)	Time (h)	Orientation ^a
I Proof Test	none	518	5000	10,000	LT
II Proof Test	600 h @ 518°F 3500 psi	350	8000	10,000	LT
III Design Data	none	500	TBD(0.2% Creep) ^b	10,000	LT
IV Design Data	none	350	TBD(0.2% Creep) ^b	10,000	LT

^aLT = long transverse.

^bTo be determined.

Table 4. Creep Tests^a on 2219-T6 Forging

Test	Specimen No. ^b	Temp (°F)	Stress (ksi)	Creep, ϵ_p (%)	Time, t (h)	Rate, $\dot{\epsilon}_m$ (h^{-1})	Status
I, Proof	LT-11	518	5.0	0.116	955	6.6×10^{-7}	Running
II, Proof	LT-6	518	3.5	0.084	597	c	---
	LT-6	350	8.0	0.024	907	1.5×10^{-7}	Running
III, Design	LT-7	500	9.5	0.371	979	2.0×10^{-6}	Discont.
III, Design	LT-12	500	8.2	0.280	1267	1.2×10^{-6}	Discont.
III, Design	LT-17	500	7.7	0.259	1145	1.5×10^{-6}	Running
III, Design	LT-9	500	6.0	0.070	163	c	Running
III, Design	LT-14	500	5.0	d			Running
IV, Design	LT-8	350	7.0	0.151	258	c	Running
IV, Design	LT-13	350	5.8	d			Running
Preliminary	L-1	500	9.5	0.154	1026	4.6×10^{-7}	Discont.
Preliminary	L-2	350	8.0	0.221	1145	1.5×10^{-7}	Discont.

^aConducted in air.

^bLT = long transverse orientation, L = longitudinal.

^cIn primary creep stage.

^dJust started.

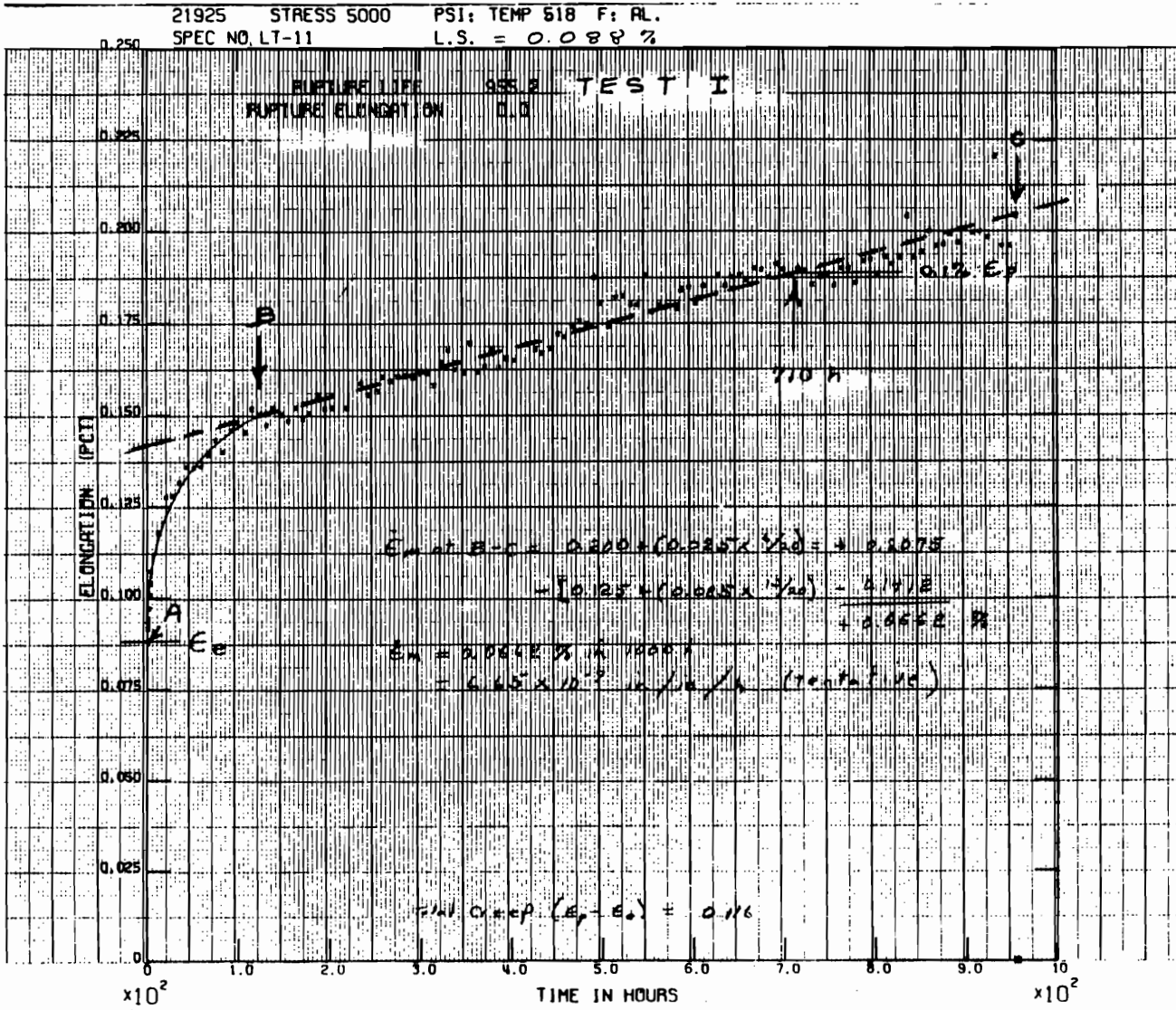


Fig. 1. Proof Test I (Space Flight). Strain = (a) 0.06% primary creep (AB) plus (b) 0.056% secondary creep (BC) at rate (ϵ_m) of $6.6 \times 10^{-5}\%/h$. Secondary creep in 10,000 h would be 0.66%.

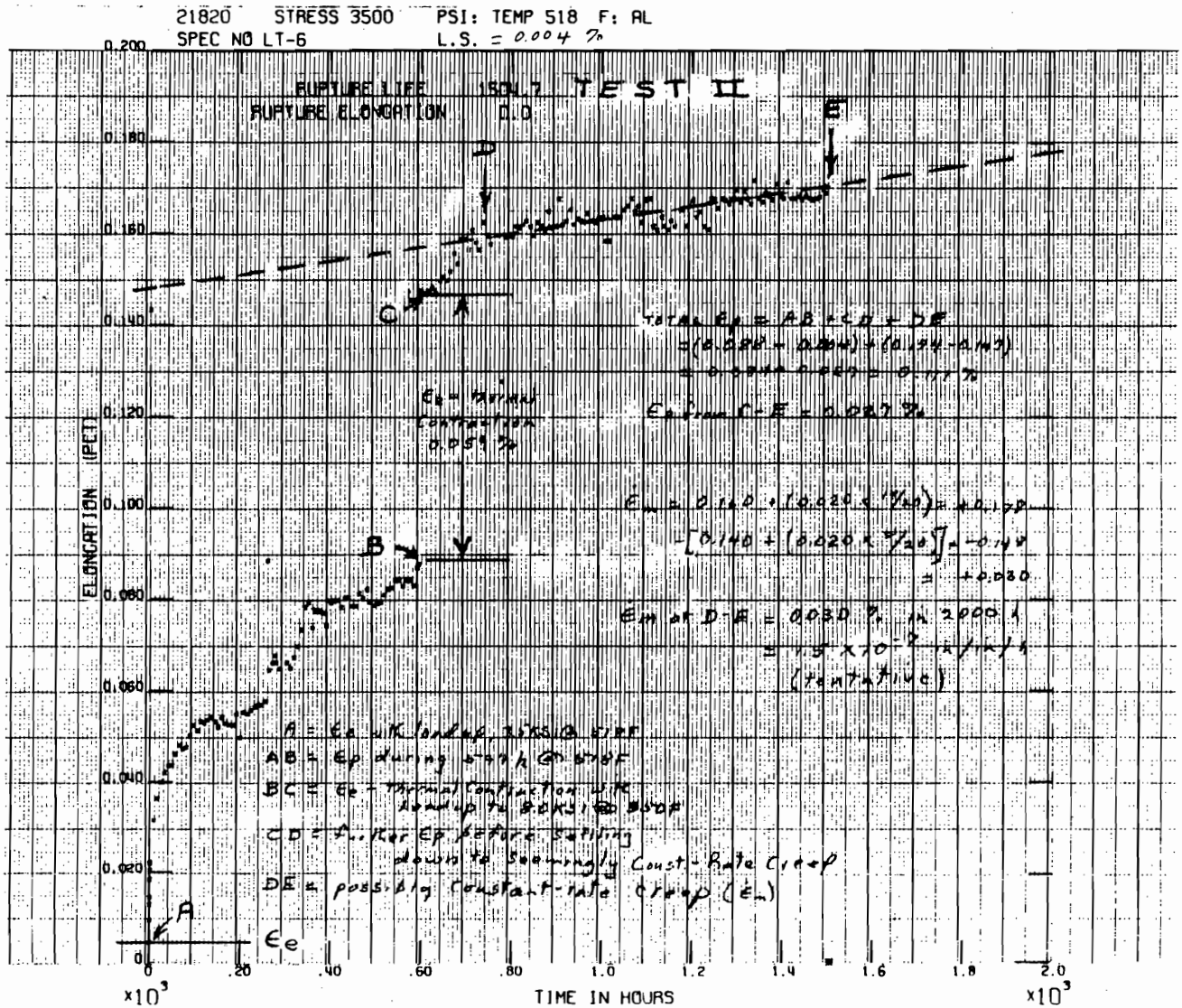


Fig. 2. Proof Test II [Ground Test (AB) and Storage (CDE)]. Strain = (a) 0.085% primary creep (AB + CD) plus (b) 0.01% secondary creep (DE) at rate ($\dot{\epsilon}_m$) of $1.5 \times 10^{-5}\%/h$. Secondary creep in 10,000 h would be 0.15%.

steady state, for which $\dot{\epsilon}_m$ is a low $1.5 \times 10^{-7}/h$. It is significant to note that the earlier aging (A-B) dissipates the bulk of the primary creep, leaving only about 0.01% (C-D) to be dissipated during the storage stage. Just as the aging stage acted to remove primary creep from the storage phase, so it would appear that the combined age-storage may remove primary creep from the flight stage (condition I) that follows upon the storage (condition II). This suggests that the pretest aging phase should be manipulated to remove the primary creep as much as possible and that stresses during storage and flight should be controlled to sufficiently limit creep strains, which in turn would then be in their minimum creep rate stages. The creep graphs for the five tests initiated to provide data for design curves at 500°F (Design III, Table I) were marked to show times for 0.1 and 0.2% creep, from which the preliminary design curves shown in Fig. 3 were prepared. This figure includes design curves for 2219-T6 aluminum forgings developed from data obtained from Alcoa, New Kensington (by private communication), for comparison. Note that our 0.1 and 0.2% curves for long transverse (LT) specimens fall about 1 to 2 ksi units below the corresponding Alcoa curves. On the other hand, our data points obtained from a longitudinal (L) specimen (L-1, Table 2) fell extremely close to the latter curves. Thus it is possible that the Alcoa data is for the longitudinal direction although this information was not given.

Whereas the data gathered thus far in support of the 500°F design curves are gratifying, it remains to be seen whether the curves will remain linear out to 10,000 h. To help resolve this question, a test was initiated at 5.0 ksi (LT-14), which lies slightly below the 0.1% curve at the 10,000 h mark.

Two creep tests were started to get initial points on the 350°F design curves (LT-8 and LT-13, Table 4). The 0.151% strain obtained in 258 h in the test loaded to 7.0 ksi stress is very high in comparison to the strain obtained at 500°F under a comparable stress-time condition. A manifestation of this behavior was experienced in the preliminary tests conducted on longitudinal specimens (L-1 and L-2, Table 2). Note in these creep experiments (conducted at 350 and 500°F for approximately 1000 h), that the test performed at the lower temperature gave a substantially greater amount of strain and did so in spite of having been loaded to a much lower stress. This suggests that the 350°F design curves we develop, paradoxically enough, will probably fall below the 500°F curves. This most unusual behavior is believed to be associated with basic differences in primary creep behavior at the two respective temperatures.

Testing will continue, focusing attention on the degree of linearity of the 500°F design curves on to times of 10,000 h and the relationship of the minimum creep rate with stress level. The testing at 350°F will be expanded.

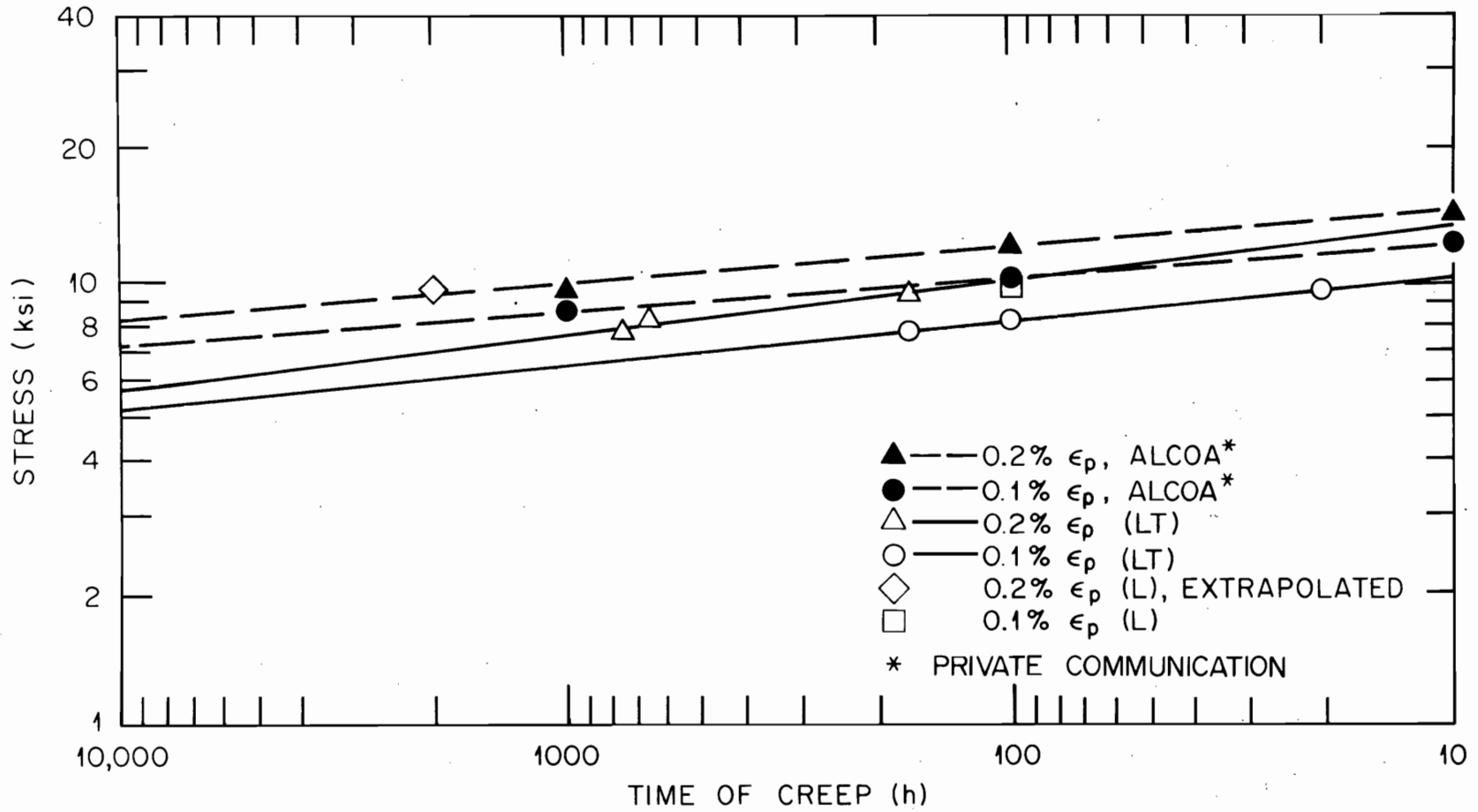


Fig. 3. Comparison of design curves of 2219T6 forgings for 0.1 and 0.2% creep at 500°F. Based on data to 1000 h.

Important Meetings

1. R. L. Heestand and R. H. Cooper attended the GPHS review meeting on June 4, 1980, at DOE/HQ, Germantown, Maryland.

2. A critical review of CBCF-3 fabrication and properties for GPHS program was held at ORNL on June 13, 1980. In attendance were R. L. Heestand, G. W. Brassell, G. C. Wei, R. L. Beatty, R. J. Beaver, A. C. Schaffhauser, R. H. Cooper, and J. Pidkowicz of DOE/ORO.

3. A. C. Schaffhauser attended the GPHS critical review meeting on June 27, 1980, at DOE/HQ, Germantown, Maryland.

FLIGHT SYSTEMS HARDWARE

(Activity AE 15 20 00 0, WPAS 01322)

D. E. Harasyn

The objective of this task is to supply Mound Facility with flight quality hardware components for use in the assembly of isotope heat sources. The major activity is on fabrication of iridium alloy forming blanks for isotope fuel capsules along with iridium foil for vents, decontamination covers, and weld shields. We have completed fabrication of iridium for the Galileo mission MHW heat source and have initiated fabrication of 1255 iridium blanks and associated foil for Solar-Polar Mission General Purpose Heat Source for delivery in FY 1980 and FY 1981. The task on fabrication of carbon-bonded carbon-fiber (CBCF) thermal insulation for Light Weight Radioisotope Heating Units (LWRHU) has been deleted due to selection of pyrolytic graphite for the application.

Iridium Forming Blank Fabrication (D. E. Harasyn)

No forming blanks were shipped to MRC in June. Of the 266 blanks for GPHS production that were to have been shipped by the end of June (June 1, 1980, Integrated Master Schedule), 219 have been shipped. Approximately 50 blanks are ready for shipment pending completion of the visual inspection. The criteria for the visual inspection has been under discussion among MRC, ORNL, DOE, and GE and is expected to be revised to more precisely define acceptable surface flaws. The uncertainty in defining acceptable pits and crack-like discontinuities in the surface of bare rolled blanks has been the primary factor delaying shipment.

New criteria for the visual inspection of forming blanks has been proposed by ORNL as follows:

1. Any surface discontinuity, including pits, deeper than 50 μ is cause for rejection.
2. Surface inclusions visible at 30X are cause for rejection.
3. There shall be no accumulation of pits or other surface discontinuities greater than 25 μ deep whose combined area exceeds 1% of a 4.6 mm diam area within any 4.6 mm diam area.

Impact data to support this specification were presented in last month's Highlights under "Characterization of DOP-26 Ir-0.3% W Production Sheet." Inspection of 30 blanks from the lot L276-281 against this criteria resulted in no rejects. At the meeting on the QA of GPHS iridium clad inspection criteria at MRC on June 19 and 20, GE proposed a specification which would reject blanks containing pits deeper than 25 μ or larger than 100 μ diam. None of the 30 blanks from L276-281 could meet this specification. From this we can conclude that should the GE proposed specification be adopted, surface grinding will be required for all GPHS forming blanks.

Meetings

D. E. Harasyn, R. J. Beaver, and R. H. Cooper, Jr. attended meeting on QA of GPHS Iridium Clad Inspection Criteria on June 19-20, 1980, at MF.

MATERIALS TECHNOLOGY SUPPORT

(Activity AE 15 35 00 0, WPAS 01495)

C. T. Liu

The primary objective of this task is to characterize and improve the metallurgical and mechanical properties of noble base alloys, mainly DOP-26 (Ir-0.3% W doped with 60 ppm Th and 50 ppm Al), to meet the requirements of cladding material in radioisotope heat resources for the Galileo and Solar-Polar space missions. The current efforts are concentrated on four areas: (1) to characterize the impact properties of Ir alloys in the temperature range 800–1400°C, (2) to improve the low-temperature impact properties of welds in the DOP-26 alloy, (3) to identify the mechanism and sources that degrade the mechanical and metallurgical properties of doped Ir alloys under heat-source environments, and (4) to develop ductile high-temperature alloys acceptable for future flight missions.

Effect of Oxidizing Environment on GPHS Impact Temperature Margin
(C. T. Liu)

Long-term exposure of DOP-26 sheet specimens to low-pressure oxygen (1.3×10^{-3} Pa) has previously shown to cause external oxidation of thorium and thorium depletion at near surface grain boundaries. This thorium depletion unpins the grain boundaries which in turn results in enhanced growth of near surface grains. Based on the measured depth of thorium depletion and diffusivity of thorium along grain boundaries, we calculated the average grain size across the 0.64-mm-thick DOP-26 specimens after 6-month exposure to oxygen in the temperature range 1250 to 1400°C. The calculated results were reported in the Technical Highlights of Space and Terrestrial Systems Programs at ORNL for October, 1979. Because the low-temperature (<110°C) impact data for oxygen-exposed DOP-26 specimens are not available at present time, we estimate the minimum allowable impact temperature* and impact temperature margin based on the enhanced grain growth and the impact data obtained from vacuum-annealed specimens. The results are presented in Tables 5 to 8 together with those estimated by Fairchild Industries based on ORNL vacuum-annealed data. As compared with anneal in vacuum, the 6-month exposure to low-pressure oxygen lowers the impact-temperature margin by 40°C at a normal operation temperature of 1331°C. It should be noted that the results for oxygen exposure are preliminary and needed to be verified by impact of oxygen-exposed specimens as a function of temperature.

*Based on 20% local-strain goal and 10% uniform-strain criterion.

Table 5. Orbit-Decay Temperature Margin^a (°C) – Effect of Axial Gaps

Normal Operating Temperature	1331			
Peak Reentry Temperature	1426			
Grains Per 0.025 in. Wall	12 (Vacuum)		9 (Oxygen)	
Minimum Allowable Impact Temperature				
20% Local-Strain Goal	975		1015	
10% Uniform-Strain Criterion	875		920	
Axial Gaps (Total)	0		.007%	
Air Conductance	<u>100%</u>		<u>50%</u>	
Impact Temperature	999		1028	
Impact Temperature Margin:				
Versus Goal		<u>Vacuum</u>	<u>Oxygen</u>	<u>Vacuum</u>
Versus Criterion		24	-16	53
		124	+79	153
				108

^aBased on APL's 120% heating factor.

Table 6. Orbit-Decay Temperature Margin — Effect of GIS-To-As Fit
(Comparison of FI and BCL Results)

GIS-To-As-Fit	Loose						Snug					
	FI		BCL				FI		BCL			
Analyst	SAT		SAT		FOS		SAT		SAT		FOS	
Hypersonic Attitude ^a	SAT		SAT		FOS		SAT		SAT		FOS	
Clad Temperature, °C ^b												
Normal Operation	1331		1332		1332		1301				1306	
Reentry Peak	1426		1422		1387		1408				1409	
Impact	999 ^c		961		965		965				899	
Minimum Allowable ^d	975 1015		974 1015		974 1015		940 975				945 980	
Margin	(vac)(oxy)		(vac)(oxy)		(vac)(oxy)		(vac)(oxy)				(vac)(oxy)	
Versus 20% Local-Strain Goal	24	-16	-13	-54	-9	-50	25	-10			-46	-81
Versus 10% Strain Criterion	124	+79	87	+41	91	45	125	97			54	24

^aSAT, single-axis tumbling, FOS = face-on stable.

^bBased on APL's 120% heating factor.

^cWithout credit for axial gaps.

^dBased on 20% local-strain goal.

Table 7. Orbit Decay Temperature Margin –
Effect of CBCF Density

Density (gm/cc):	<u>0.20</u>	<u>0.28</u>
Temperatures, °C:		
Normal Operation	1331	1309
Reentry Peak	1426	1420
Impact ^a	999	968
Minimum Allowable ^b	975 1015 (vac)(oxy)	950 980 (vac)(oxy)
Margin ^c	24 -16	18 -12

^aBased on APL's 120% heating factor.

^bWithout credit for axial gaps.

^cBased on 20% local-strain goal.

Table 8. Prompt Reentry Temperature Margins^a (°C)

Reentry Angle	<u>-5.3°</u>	<u>-5.1°</u>	<u>-5.037°</u>
Normal Operating Temperature	1331	1331	1331
Peak Reentry Temperature	1584	1574	1533
Grains Per 0.025" Wall	22	22	22
Minimum Allowable Impact Temperature	870	870	870
Impact Temperature	1048	1000	942
Temperature Margin	178	130	72

^aBased on APL's 120% heating factor.

Effect of Test Temperature on Tensile Properties of As-Rolled DOP-26 Production Material (C. T. Liu and D. E. Harasyn)

Tensile properties of as-rolled DOP-26 production material were measured as a function of test temperature to 900°C. The purpose of this test is to determine the test temperature which can be best used to perform deep drawing of GPHS cups. Tensile specimens were punched from the sheet L-216 and edges of the gage section were machined by a grinding process. Three hardness indentations were made in the gage section of each specimen for measurement of uniform and fracture strains. The tensile results are shown in Figs. 4 and 5. The tensile strength decreases with test temperature, and the yield strength shows a sharp drop around 550°C (Fig. 4). The uniform strain in Fig. 5 shows an initial increase with temperature, followed by a decrease. The maximum uniform strain is located around 600°C. In contrast, the reduction of area increases sharply with test temperatures above 550°C and reaches 45% at 900°C. D. E. Harasyn has found that DOP-26 blanks can be successfully drawn into GPHS cups at temperatures above 550°C. Correlation of the deep-draw result with the ductility data suggests that it is the reduction of area which possibly controls the drawability of DOP-26 alloy.

Effect of Stress-Relief Temperature on Room-Temperature Tensile Properties of DOP-26 Production Material (D. E. Harasyn and C. T. Liu)

Tensile properties as a function of stress relief temperature for cold worked DOP-26 production material are shown in Fig. 6. These data were obtained from tensile samples which were punched from L-218 and L-3 sheets which had been bare rolled to final thickness (0.6 mm). The samples were acid cleaned and then annealed in vacuum for 1 h at the temperatures indicated. Hardness impressions were made in the gage lengths for strain measurement. Crosshead speed was 3 mm/min.

Cold worked DOP-26 shows very little tensile ductility in the as-rolled condition and after stress relieving at 600 or 700°C. Stress relieving above 700°C results in a steady increase in total elongation and a decrease in yield stress. The fracture stress remains essentially constant at 1250 MPa for all tests. The reduction of area for all samples was too small to measure accurately in all but the most ductile sample. These data suggest that the fabrication of cold worked DOP-26 can be improved by proper stress-relief treatment.

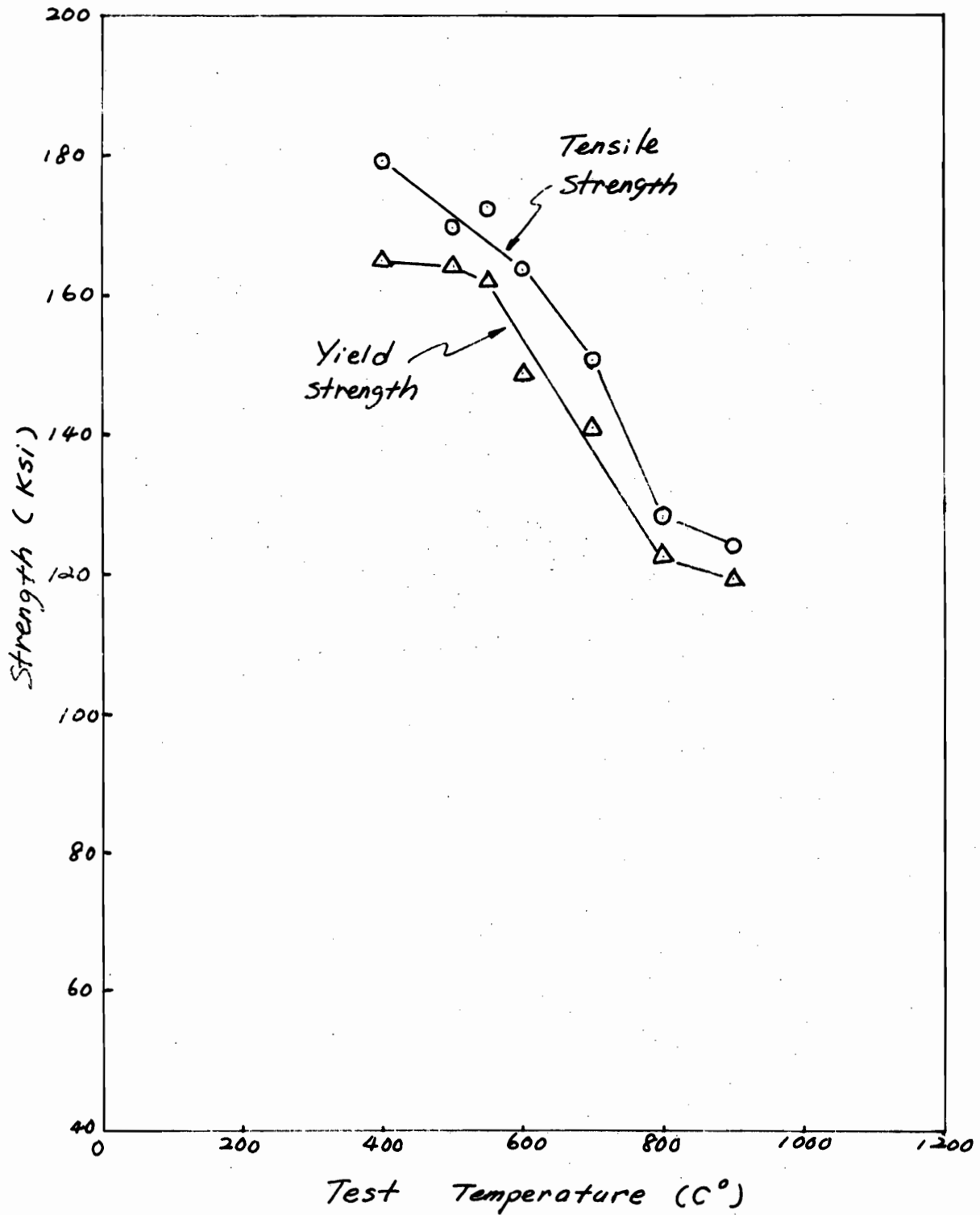


Fig. 4. Yield and Tensile Strength of the Stress-Relieved DOP-26 Sheet (L-216) as a Function of Test Temperature.

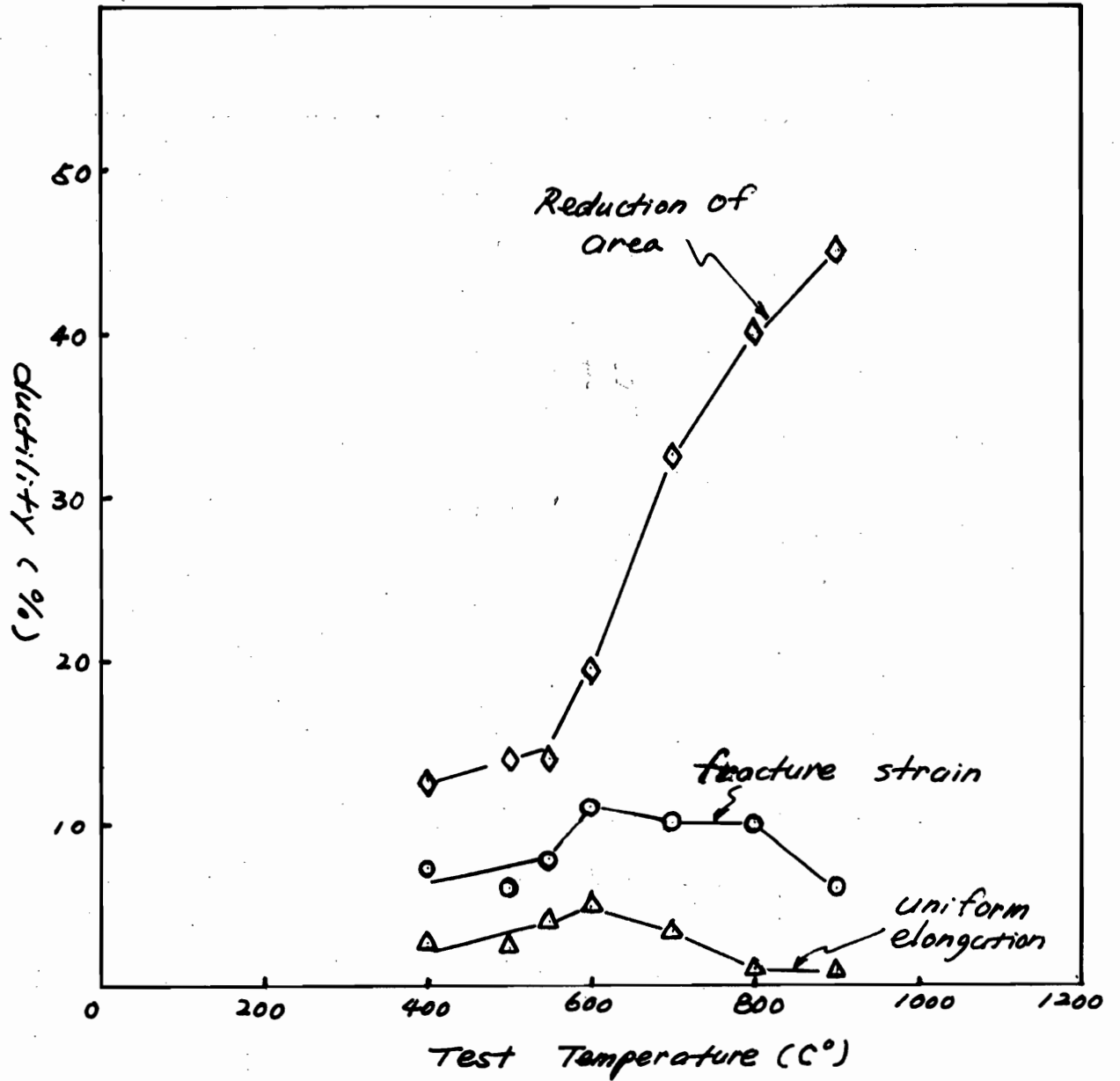


Fig. 5. Tensile Ductility of the Stress-Relieved DOP-26 Sheet (L-216) as a Function of Test Temperature.

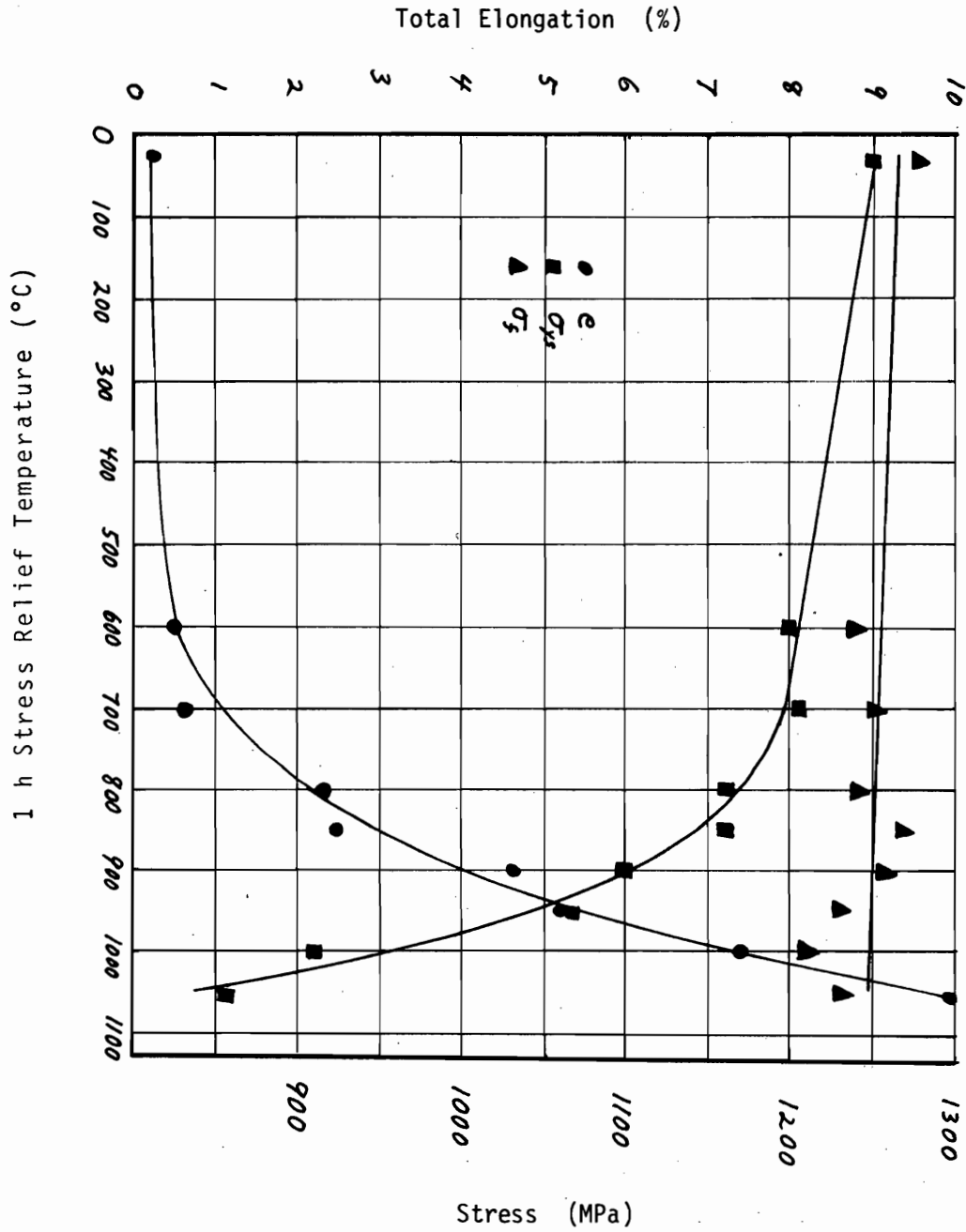


Fig. 6. Room Temperature Tensile Properties of Cold Worked DOP-26 Alloy vs Stress-Relief Temperature.

Slow Strain Rate Tensile Properties of Pt-30 Rh Alloy (J. R. Keiser)

The tensile properties of Pt-30 Rh have been measured between -196 and 1515°C at a strain rate of 0.2 min^{-1} . The results are plotted in Fig. 7. These results show that the ultimate tensile strength and 0.2% yield strength approach similar values at high temperatures. The measured values of the elongation show two ductility minima at high temperatures; these minima may be real or may be due to scatter in the limited number of samples tested.

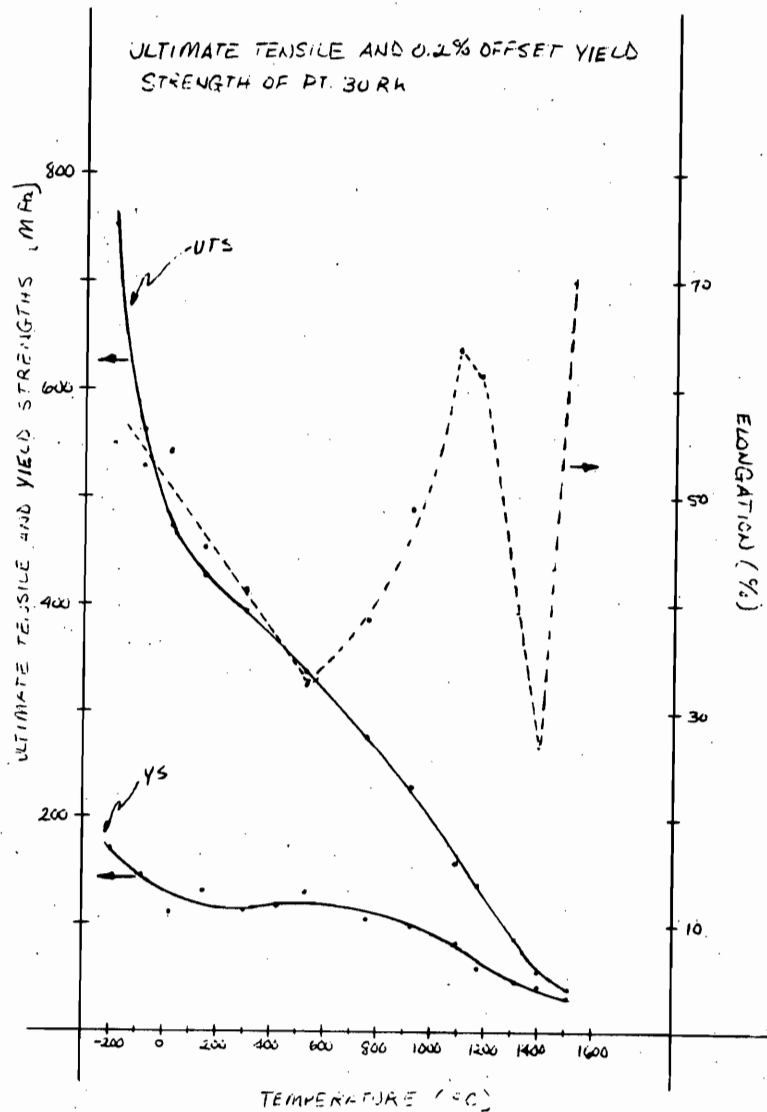


Fig. 7. Plot of Tensile Properties of Pt-30 Rh as a Function of Test Temperature.

Bonding of $(\text{Cu,Ag})_2\text{Se}$ to W-25% Re (D. E. Harasyn and G. C. Wei)

The purpose of these experiments was to find the proper conditions of heat and pressure that would metallurgically bond the as-cast $(\text{Cu,Ag})_2\text{Se}$ P-leg to its sandblasted W-25% Re cap. The deterioration the contact between the hot end of the $(\text{Cu,Ag})_2\text{Se}$ P-leg and W-25% Re cap was identified as the primary factor responsible for the erratic behavior and degradation of the output power of some selenide testing modules. The objective of the present study is to improve the hot end bond of the as-made P-leg assembly and to eliminate the deterioration of the contact in service.

Four sets of P-legs (6.22 mm diam \times 10.2 mm long), cast at ORNL, and caps (8.1 mm max diam \times 0.51 mm thick), supplied by 3M Company, were available for experimentation. Each P-leg and cap set were cleaned ultrasonically in ethanol. A single set was placed in an alignment fixture and then heat treated 1 h at the temperatures listed in Table 9. The alignment fixtures was made from POCO graphite and was intended to align the axes of the P-leg components to within about 0.10 mm. A plunger was provided to apply a load on the end of the selenide cylinder opposite the cap. A tungsten element vacuum hot press furnace was used for the heat treatments. Pressure in the furnace was maintained near 1×10^{-3} Pa during each run. Heatup and cooldown times were typically 4 h. Pressing conditions and results are shown in Table 9.

The loads listed in Table 9 are thought to be accurate only to within 20N (5 lb). The very low loads required for these experiments necessitated a balance system to counteract the force of atmospheric pressure on the push rod of the hot press furnace. Because there was substantial binding in the O-ring seal of the furnace push rod, the force of atmospheric pressure on the rod could not be very accurately determined. The sample run at a load of 9N (2 lb) had a dead weight on top of it, thus, circumventing the furnace push rod, and this load is therefore meaningful.

The quality of the bond was determined simply by applying finger pressure to the heat treated assembly so as to peel the cap off. Either the cap came off easily (poor) and no reaction between selenide and W-Re was observed, or else the cap could not be separated from the P-leg without fear of breaking one of the components (good). Longitudinal cross sections of both a good and poor bond were examined at high magnification under polarized light. (The dissimilarity of the two materials prevented the use of etchants). No reaction layer could be observed in either sample.

Deformation of the selenide occurred in most of the heat treatments. The selenide was restrained over 90% of its surface by the graphite fixture. Where there was no restraint, the selenide would often extrude. We noted that after heating to 1050°C, small dimples appeared on the wall of the selenide cylinder. This phenomenon seemed of little consequence and was not investigated.

It may be concluded that the as-cast $(\text{Cu,Ag})_2\text{Se}$ P-leg can be tightly bonded to the sandblasted W-25%Re cap by applying a load of about 50N to the assembly while heating under vacuum at 1050°C . Slight extrusion of the selenide can be expected depending upon the amount of restraint afforded by the alignment fixture. This flash can easily be removed.

One set (sample #4), bonded at 1050°C and 50N, has been given to 3M Company for long-term testing.

Table 9. Summary of Pressure/Heat Treatments Used to Bond (Cu,Ag)₂Se to W-25% Re

P-leg Sample	Bonding Conditions		Bond Quality	Selenide Deformation	P-leg/cap Disposition
	Temperature (°C)	Load (N)			
1	850	440 (100 lb)	poor	yes	re-used
2	900	0	poor	no	re-used
2	900	530 (120 lb)	poor	yes	to metallography
1	1050	160 (35 lb)	good	yes	to metallography
3	1050	50 (11 lb)	good	yes	to 3M, selenide fractured during machining to remove flash at ORNL
4	1050	50 (11 lb)	good	yes	to 3M Co.
4	1050	9 (2 lb)	poor (very slightly reaction observed)	no	re-used

ISOTOPE FUEL DEVELOPMENT

(Activity AE 15 35 00 0, WPAS 02314)

R. S. Crouse

 $^{90}\text{SrF}_2$ Compatibility (R. S. Crouse)

Microprobe examination of the 30,000 h test of $^{90}\text{SrF}_2$ compatibility has not begun because of the demands of other programs on the time of the personnel.

At the request of H. T. Fullam, Battelle-PNL, we have agreed to metallographically examine the end cap of a capsule containing $^{90}\text{SrF}_2$ from Rockwell-Hanford. Lars Edvaldson suspects some kind of defect in the cap and wishes us to look for it. The cap has been removed at FPD and shipped to Bldg. 3525.

TERRESTRIAL RADIOISOTOPE APPLICATION DEVELOPMENT

(Activity AE 15 35 00 0, WPAS 01367)

F. N. Case, K. W. Haff, and F. J. Schultz

Cesium-137 Low Solubility Compounds

The leaching equipment, including the Soxhlet extractors, water lines, etc., was transferred into the hot cell and reassembled. The previously sectioned fully loaded ^{137}Cs aluminosilicate pellets were placed in their respective sample cups and the leach testing begun. The first two samples from each Soxhlet extractor are given in Table 10.

Table 10. Leach Rates of Fully Loaded ^{137}Cs Aluminosilicate Pellets

Sample No.	Accumulated Leaching Period (days)	Leach Rate ($\text{g}/\text{cm}^{-2}\text{day}^{-1}$)
5-1	1	2.456×10^{-4}
5-2	3	2.783×10^{-4}
6-1	1	2.213×10^{-4}
6-2	3	3.275×10^{-4}
7-1	1	1.281×10^{-4}
7-2	3	1.374×10^{-4}
8-1	1	3.075×10^{-4}
8-2	3	4.563×10^{-4}

Leach testing of the three sections of tracer level ^{137}Cs aluminosilicate pellets continued this month. The leach rates of each pellet section are given in Table 11. The previously reported leach rates for the tracer level pellet sections were re-evaluated and found to be low by a factor of 3/0.345. This factor is derived from the isotopic fraction of ^{137}Cs in the powder and the ^{137}Cs -containing powder being diluted 3 to 1 with cold cesium-containing powder. Thus the total cesium leached from each tracer level pellet section is the previously reported rate multiplied by a correction factor of 8.70.

Table 11. Leach Rates of Tracer Level ^{137}Cs Aluminosilicate Pellets

Sample No.	Accumulated Leaching Period (days)	Leach Rate ($\text{g}/\text{cm}^{-2}\text{day}^{-1}$)
1-8832	368	1.72×10^{-4}
2-8832	368	6.60×10^{-5}
3-8832	368	1.51×10^{-4}

As one can see from a comparison of Tables 10 and 11, the leach rate results from the fully loaded ^{137}Cs aluminosilicate pellets are very similar to those of the tracer level pellets. It would be premature to draw any conclusions or predict any relationships from these preliminary results.

Two fully loaded ^{137}Cs aluminosilicate pellets were transferred into the hot cell. These unsectioned pellets will be static leach tested with distilled water to determine the leach rates of uncut, whole pellets. The results will be compared with those obtained from the sectioned pellets.

Krypton-85 Light Source Development

Eight lights for demonstration in July were completed and shipping containers fabricated to meet DOT requirements.

The base units for the lights were redesigned to incorporate a lead shield to replace a portion of the brass. This provided a 5 lb weight reduction for each unit.

Each unit was loaded with 10 Ci of ^{85}Kr enriched to an average of 35%. Plans to load one or two of the units with 30 Ci had to be delayed due to the shortage of enriched ^{85}Kr . Future plans are to evaluate both enriched and normal ^{85}Kr at various loadings up to 30 Ci. Shielding problems at the light pipe are anticipated at the higher loading and may require a design modification to increase the diameter of the light pipes.

A tritium taxi marker was prepared for demonstration along with the ^{85}Kr lights.

Design changes needed to meet Air Force requirements will be defined after the July demonstration.

BENEFICIAL APPLICATIONS OF RADIATION TECHNOLOGY

(Activity AE 15 35 00 0, WPAS BART001)

C. S. Sims

All review comments on the April 25, 1980 draft Cs-137 irradiation technology program assessment document were received by June 16. Work on the resolution of the 118 comments began and continued throughout the report period.

Dr. Richard L. Tyndall, a microbiologist with an exceptionally strong background in virology, has been identified to take the principal sublead for biological-related technology in the BART program. Dr. Tyndall will report to Dr. Sims.

The BART program manager (C. S. Sims) joined S. B. Ahlstrom (CH2M HILL) and J. S. Sivinski (Sandia) in Provo, UT at a June 3 meeting of the City Commission to hear a CH2M HILL presentation related to locating a sewage sludge irradiation demonstration plant in Provo. Merrill Bingham, the Director of Provo's Water and Waste Water Office, and the Commission expressed interest in such an endeavor. It was proposed that the plant be 85% funded under the Environmental Protection Agency's innovative and alternative technology construction grants program with the remainder coming from the city and the state.

CH2M HILL and BART program personnel met in Boise, ID on June 25 to discuss the status and future directions of the program. The discussions were mutually beneficial and some of the results will be reflected in the BART program plan.

INTERNAL DISTRIBUTION

- | | | | |
|------|------------------|--------|-----------------------------|
| 1. | E. E. Bloom | 25. | J. W. Koger |
| 2. | C. R. Brinkman | 26. | H. Inouye |
| 3. | J. A. Carter | 27. | E. Lamb |
| 4. | F. N. Case | 28. | C. T. Liu |
| 5-9. | R. H. Cooper | 29. | D. L. McElroy |
| 10. | R. S. Crouse | 30. | C. D. Montgomery |
| 11. | J. E. Cunningham | 31. | T. K. Roche |
| 12. | S. A. David | 32. | A. C. Schaffhauser |
| 13. | J. H. DeVan | 33. | C. S. Sims |
| 14. | R. G. Donnelly | 34. | G. M. Slaughter |
| 15. | W. P. Eatherly | 35. | J. O. Stiegler |
| 16. | J. I. Federer | 36. | V. J. Tennery |
| 17. | G. M. Goodwin | 37. | D. B. Trauger |
| 18. | K. W. Haff | 38. | G. C. Wei |
| 19. | J. P. Hammond | 39. | J. R. Weir, Jr. |
| 20. | D. E. Harasyn | 40. | C. L. White |
| 21. | W. O. Harms | 41-45. | Laboratory Records |
| 22. | R. L. Heestand | 46. | Laboratory Records, ORNL RC |
| 23. | M. R. Hill | 47. | ORNL Patent Office |
| 24. | J. R. Keiser | | |

EXTERNAL DISTRIBUTION

48-59. DOE Space and Terrestrial Systems Division, Washington, DC 20545

G. L. Bennett	J. J. Lombardo
R. C. Brouns	R. B. Morrow
F. M. Dieringer	P. A. O'Riordan
N. Goldenberg	W. C. Remini
J. S. Griffo	B. J. Rock
W. D. Kenney	C. O. Tarr

60-61. DOE Albuquerque Operations Office, P.O. Box 5400,
Albuquerque, NM 87115

D. K. Nowlin
D. Plymale

62-63. DOE Oak Ridge Operations Office, P.O. Box E, Oak Ridge, TN 37830

J. A. Lenhard
J. Pidkowicz

- 64-65. DOE San Francisco Operations Office, 1333 Broadway, Wells Fargo Building, Oakland, CA 94612
- L. Lanni
W. L. Von Flue
- 66-67. DOE Savannah River Operations Office, P.O. Box A, Aiken, SC 29801
- W. T. Goldston
W. D. Sandberg
68. DOE Dayton Area Office, P.O. Box 66, Miamisburg, OH 45342
- H. N. Hill
69. Air Force Weapons Laboratory, Kirtland Air Force Base, DYUS, Albuquerque, NM 87116
- Michael Seaton
- 70-71. Battelle Columbus Laboratories, 505 King Ave., Columbus, OH 43201
- E. L. Foster
I. M. Grinberg
- 72-73. E. I. du Pont de Nemours, Savannah River Plant, Aiken, SC 29801
- R. A. Brownback
W. R. Kanne
- 74-75. E. I. du Pont de Nemours, Savannah River Laboratory, Aiken, SC 29801
- R. L. Folger
R. H. Tait
- 76-77. Fairchild Industries, 20301 Century Blvd., Germantown, MD 20767
- M. Eck
A. Schock
78. General Atomic Co., P.O. Box 81608, San Diego, CA 92138
- N. B. Elsner
- 79-81. General Electric Co., Valley Forge Space Center, P.O. Box 8048, Philadelphia, PA 19101
- V. Haley
R. J. Hemler
C. W. Whitmore

- 82-84. Jet Propulsion Laboratory, California Institute of Technology,
4800 Oak Grove Drive, Pasadena, CA 91103
- R. W. Campbell
J. E. Mondt
A. E. Wolfe
85. Johns Hopkins University, Applied Physics Laboratory, Johns
Hopkins Road, Laurel, MD 20810
- J. C. Hagan
- 86-88. Los Alamos Scientific Laboratory, P.O. Box 1663,
Los Alamos, NM 87545
- S. E. Bronisz
S. S. Hecker
W. J. Maraman
- 89-91. Minnesota Mining and Manufacturing Co., St. Paul, MN 55101
- R. B. Ericson
J. D. Hinderman
W. C. Mitchell
- 92-93. Monsanto Research Corp., P.O. Box 32, Miamisburg, OH 45342
- E. W. Johnson
W. C. Wyder
94. Sundstrand Energy Systems, 4747 Harrison Ave., Rockford, IL 61101
- E. Krueger
- 95-96. Teledyne Energy Systems, 110 W. Timonium Rd., Timonium, MD 21093
- W. J. Barnett
W. E. Osmeyer

